Results in Engineering 17 (2023) 100828

Contents lists available at ScienceDirect

Results in Engineering

journal homepage: www.sciencedirect.com/journal/results-in-engineering

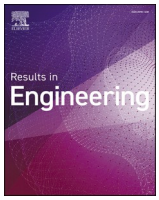

Novel deconvolution method for extreme FPSO vessel hawser tensions during offloading operations

Oleg Gaidai [a], Xiaosen Xu [b], Yihan Xing [c,*]

[a] Shanghai Engineering Research Center of Marine Renewable Energy, College of Engineering Science and Technology, Shanghai Ocean University, Shanghai, China
[b] Jiangsu University of Science and Technology, Zhenjiang, China
[c] University of Stavanger, Norway

ARTICLE INFO

Keywords:
Floating production storage and offloading (FPSO)
Monte Carlo
SBS offloading
Energy

ABSTRACT

Robust prediction of extreme hawser tensions during Floating Production Storage and Offloading (FPSO) operations is an important safety and reliability concern. Excessive hawser tension may occur during certain environmental conditions, posing an operational risk. The novel deconvolution method is proposed in this paper to provide an accurate extreme value prediction. The predicted return level values produced by the new deconvolution approach are compared with those obtained by the Naess-Gaidai method. On the basis of the suggested approach's overall performance, it is concluded that the innovative deconvolution method may give a more robust and accurate forecast of excessive hawser stress. The stated method may be used effectively at the stage of vessel design while determining appropriate vessel characteristics to reduce possible FPSO hawser stress.

1. Introduction

FPSO technology nowadays is vital for offshore petroleum and natural gas exploration. Offloading operations are indispensable parts during the whole process of oil and gas offshore production, thus playing a pivotal role in the entire FPSO operational design. For the side-by-side (SBS) offloading system FPSO and tanker are placed next to each other. The latter method is more cost-effective and practicable than tandem unloading. The focus of this study is the SBS offloading system.

In this study, the authors sought to use a generic Monte Carlo (MC)-based technique capable of addressing the majority of nonlinear effects without further simplifications beyond those intrinsic to numerical modeling itself [1–4].

The general framework of a wide range of offshore engineering applications that utilize the suggested approach includes but is not limited to a structural design, reliability assessment, risk management under realistic environmental conditions.

The novel deconvolution method was combined with a suitable class of parametric functions for analyzing the response distribution tail behaviour. Following [3], this paper extends the work of establishing an accurate method for estimating extreme hawser tension that avoids invoking the ultimate asymptotic distributions but instead tries to capture the sub-asymptotic behaviour of extreme value data if appropriate.

2. Wave statistics

Satellite-based global wave statistics were employed to generate a correct wave scatter diagram in the South China Sea region of FPSO operations; more specifically, Global Wave Statistics Online [5] data was applied.

Each sea state, (H_s, T_p) of each direction in the scatter diagram was simulated for 3 h. The random stationary sea state is characterized by the JONSWAP wave spectrum, which is the power spectral density (PSD) of the wave height $\eta(t)$, denoted by $S_\eta^+(\omega)$, is then given as follows $(\omega > 0)$

$$S_\eta^+(\omega) = \frac{\alpha g^2}{\omega^5} exp\left\{ -\frac{5}{4}\left(\frac{\omega_p}{\omega}\right)^4 + ln\,\gamma \bullet exp\left[-\frac{1}{2\sigma^2}\left(\frac{\omega}{\omega_p} - 1\right)^2 \right] \right\} \quad (1)$$

with $g = 9.81\mathrm{m/s}^2$, ω_p denoting the peak frequency in rad/s; and α, γ and σ being parameters related to the spectral shape; $\sigma = 0.07$ when $\omega \le \omega_p$,; $\sigma = 0.09$ when $\omega > \omega_p$ (see Fig. 1).

Fig. 2 presents a flow chart for the methodology applied in this paper. The latter scheme is classical for long-term extreme value or fatigue analysis.

* Corresponding author.
E-mail address: yihan.xing@uis.no (Y. Xing).

https://doi.org/10.1016/j.rineng.2022.100828
Received 15 September 2022; Received in revised form 3 December 2022; Accepted 6 December 2022
Available online 9 December 2022

Fig. 1. FPSO vessel and its multi-point mooring system.

3. Numerical modeling of SBS operation between FPSO and shuttle tanker

3.1. Parameters of vessels

Table 1 lists the primary parameters of the FPSO and the shuttle. It is expected that the FPSO is anchored using a multipoint mooring method. Fig. 3 depicts the SBS offloading system and its multi-point mooring system.

In this paper, hawser # 3, denoted as H3 in Fig. 3, has been chosen for detailed analysis since that hawser was found to be most critical, i.e. carrying maximal tension.

3.2. Numerical calculation of SBS offloading mooring system

The proximity between two vessels influences drift forces and motions. Fig. 4 schematically shows the FEM coupled panel model of FPSO along with the shuttle tanker. The details of the numerical simulation are listed below:

i) Numerical simulation considers the hydrodynamic interaction between two vessels. The effect of water depth is also considered in calculating hydrodynamic forces or moments using the Pinkster approximation [6]. Fig. 4 schematically shows the FEM coupled panel model of the FPSO and shuttle tanker. The panel size is less than 2 m, and the number of panels is about $2 \bullet 10^4$ in conducted FEM analysis.

ii) Sources of damping on a moored structure are multiple and of various natures. In lieu of actual data, equations from the Bureau Veritas [7] categorization of mooring systems for permanent offshore units may be utilized as a main technique to derive linear damping coefficients.

$$B_{xx} = 0.06\sqrt{K_{O_{xx}}(m + Ma_{xx})}, B_{yy} = 0.06\sqrt{K_{O_{yy}}(m + Ma_{yy})} \quad (2)$$

$$B_{\psi\psi} = 0.06\sqrt{K_{O_{\psi\psi}}\left[I_{\psi\psi} + \psi Ma_{\psi\psi} + (m + Ma_{yy})x_G^2\right]} \quad (3)$$

Table 1
Main particulars of the reference FPSO vessel and shuttle tanker.

Designation	Signal	Unit	FPSO	Shuttle tanker
Length overall	L_{OA}	m	235.6	207
Length between perpendicular	L_{PP}	m	225	194
Breadth	B	m	46	36
Depth	D	m	24.1	16
Draft	T	m	11	8.7
Displacement	Δ	t	104748.4	49444
Centre of gravity above base	KG	m	10.242	11.8
Centre of gravity from AP	L_{CG}	m	110	98.8

where B_{xx}, B_{yy} and $B_{\psi\psi}$ are linear damping coefficients in surge, sway and yaw.K_{Oxx}, K_{Oyy} and $K_{O\psi\psi}$ are diagonal terms of the mooring stiffness matrix $[K_O]$. $I_{\psi\psi}$ is the moment of inertia in yaw, in kg/m^2, calculated at the centre of the gravity (CoG) of the FPSO structure.

iii) Based on the Oil Companies International Marine Forum (OCIMF) data, wind and current coefficients are determined for the loaded vessel. In the time domain analysis, the JONSWAP spectrum is used to calculate wave forces on vessels. Because of the mutual effects on the FPSO and shuttle tanker, the shielding factor is also considered a reduction factor based on the CFD simulation result.

iv) The second-order drift forces have been evaluated by using a full quadratic transfer function matrix and integrating pressure of the wetted surface area of two vessels. Besides, since the far-field solution is unable to consider multiple objects separately, the near-field solution has been adopted.

v) According to American petroleum institute (API) reference rules [8] for the multi-point mooring system and SBS offloading system, the SBS offloading operation is restricted only for head sea conditions with significant wave height H_s under 2.4 m. Norwegian Petroleum Directorate (NPD) spectrum is chosen for the wind spectrum, and the wind speed at 10 m above mean sea level is 16 m/s. The current speed is 0.6 m/s. Therefore, several typical environmental conditions are selected for calculation. Fig. 5 shows the directions of winds, currents and waves for different environmental conditions.

According to American petroleum institute (API) reference rules [8] for multi-point mooring systems and SBS offloading systems, SBS offloading operation is typically restricted only for head sea conditions with significant wave height H_s under 2.4 m. Fig. 5 shows wind, current and wave directions for different environmental conditions.

Fig. 5 presents six typical sea/environmental conditions that have been chosen for numerical analysis in this paper. Ten hawsers (H_1,..,H_{10}) were arranged for the SBS offloading system, made of nylon-type ropes with a diameter of 110 mm. For details on the mooring ropes, e.g. stiffness, line lengths, damping, etc., see Refs. [9,10].

4. Results

This section discusses frequency and time domain numerical results for FPSO responses in unidirectional seas. Fig. 6 shows times series data samples and corresponding power spectral densities (PSD) in EC1. The

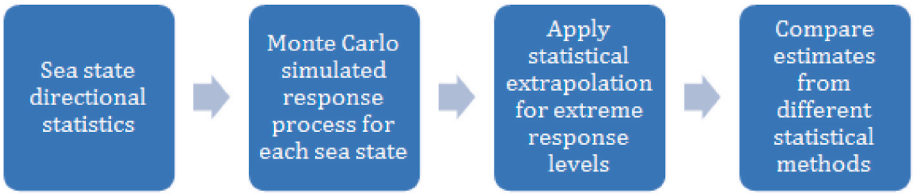

Fig. 2. Flow chart for the described methodology.

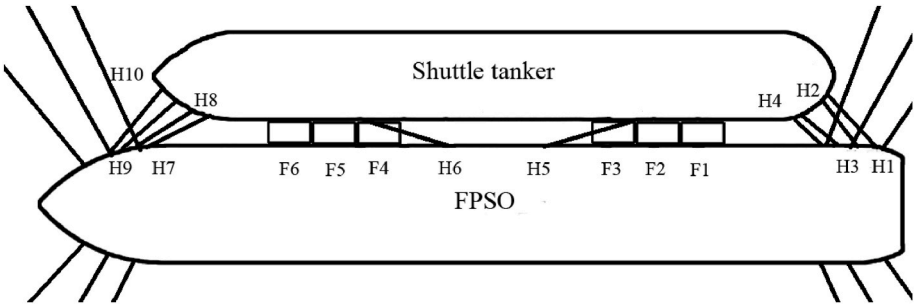

Fig. 3. The layout of the SBS offloading system and multi-point mooring system.

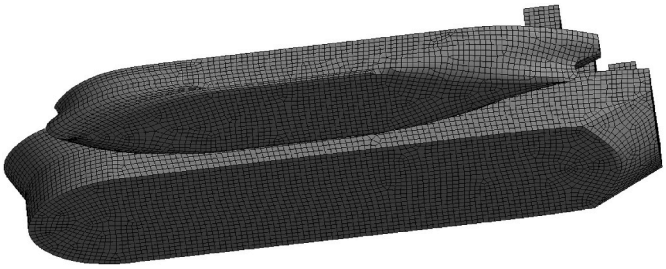

Fig. 4. FEM coupled model of the FPSO and shuttle tanker.

PSD is based on the full simulation duration of 10800 s, cutting out the initial transient time.

Fig. 7 shows the statistical characteristics of 10 hawsers tensions in different environmental conditions.

5. Novel methodology motivation

Accurate extreme value prediction is a common and challenging engineering reliability task, especially when available data is scarce. Therefore, developing novel, efficient and accurate extrapolation techniques are of great practical importance.

Consider a stationary stochastic process $X(t)$, simulated or measured over a certain period of time $0 \le t \le T$, which is represented as the sum of two independent stationary processes, $X_1(t)$ and, $X_2(t)$

$$X(t) = X_1(t) + X_2(t) \tag{4}$$

Note that this paper aims at a general methodology applicable to extreme FPSO hawser tension predictions and for a wide range of loads and responses for various green energy mechanical installations. For the process of interest $X(t)$ one may obtain marginal PDF (probability density function) p_X by two different ways

A) by directly extracting $p_X \approx p_X^A$ from the available data set, i.e. time series $X(t)$,
B) by extracting PDFs independently from the process components $X_1(t)$ and $X_2(t)$, namely p_{X_1} andp_{X_2}, then applying convolution $p_X \approx p_X^B = conv(p_{X_1}, p_{X_2})$.

Both p_X^A and p_X^B are being approximations of the target PDF p_X. Approach A) is straightforward to use, as it relies only on the available raw data set without enhancing its domain support and its probability distribution accuracy; however, approach B), if successful, would provide an estimate of the target PDF p_X with enhanced accuracy and wider PDF domain support. An advantage of using convolution in case B) is based on the fact that convolution enables extrapolation of the directly extracted empirical PDF p_X^A, without pre-assuming any specific extrapolation functional class, e.g. generalized extreme value distributions (GEV), needed to extrapolate distribution tail towards design low probability level of interest. Note that most existing extrapolation methods, widely adopted in engineering practice, rely on assuming certain extrapolation functional classes, e.g. Refs. [1–4,11,12]. To name

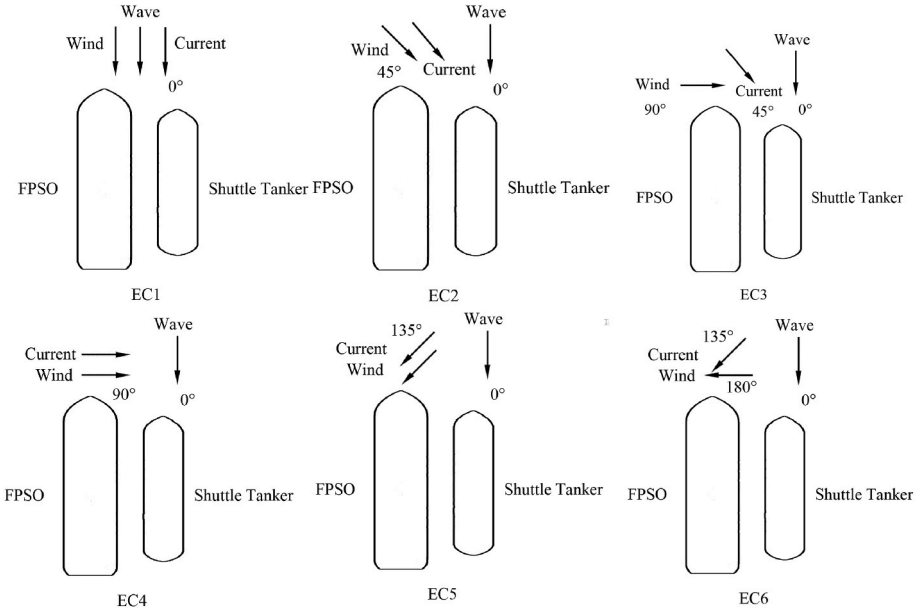

Fig. 5. Six typical environmental conditions.

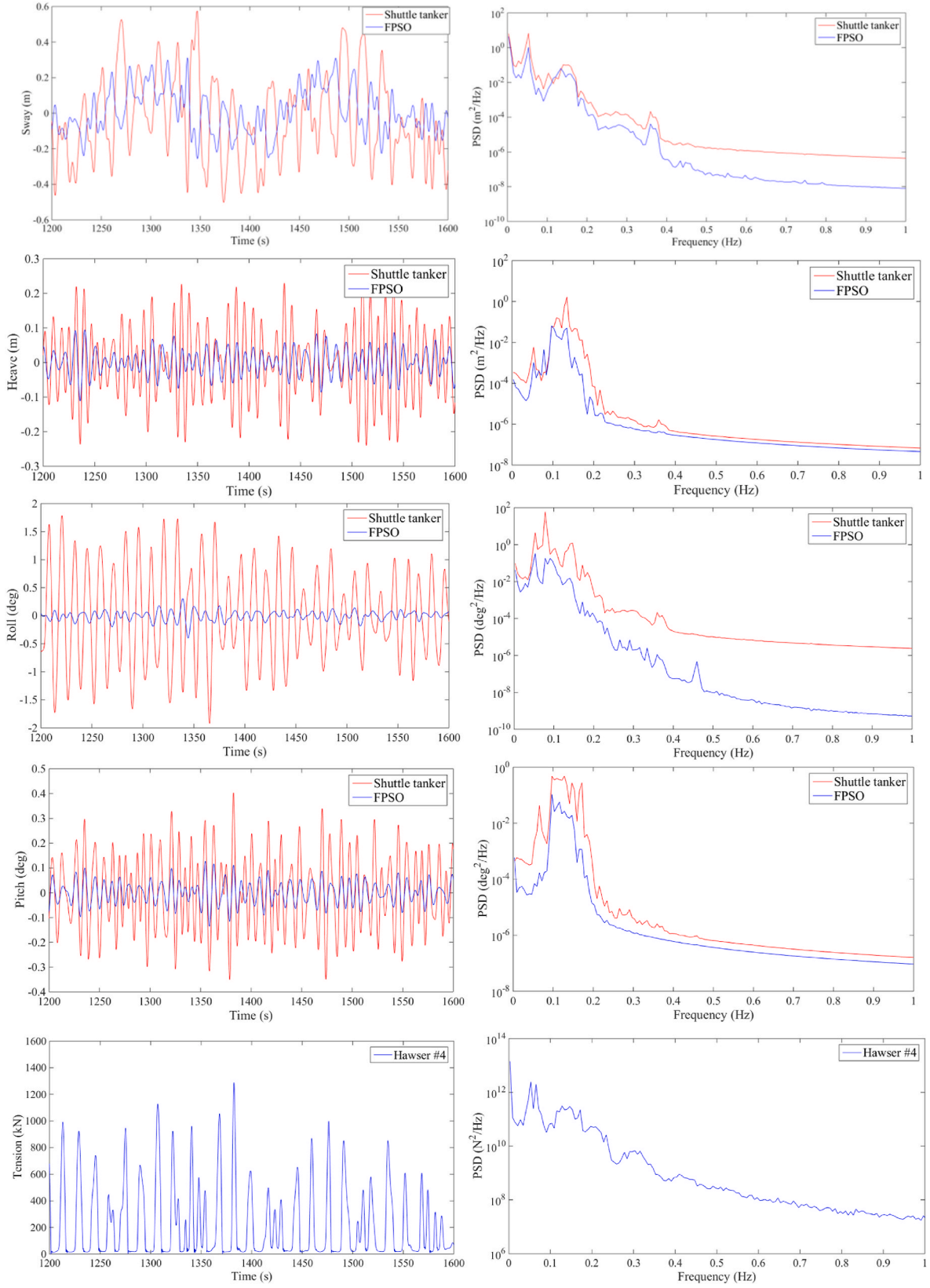

Fig. 6. Sectional time series data and power spectral densities.

some of those most popular existing methods: Pareto-based distribution peak over the threshold (POT) see, e.g. Ref. [11], Naess-Gaidai (NG) based fit used in averaged conditional exceedance rate (ACER) method, see, e.g. Refs. [1–4,11,12], bivariate ACER [9,13–17]; Weibull distribution based fit, Gumbel distribution based fit, see, e.g. Ref. [11].

The two independent component representation given by Eq. (4) is seldom available; therefore, one may look for artificial ways to estimate p_{X_1} andp_{X_2}, or in the simplest case, find two identically distributed

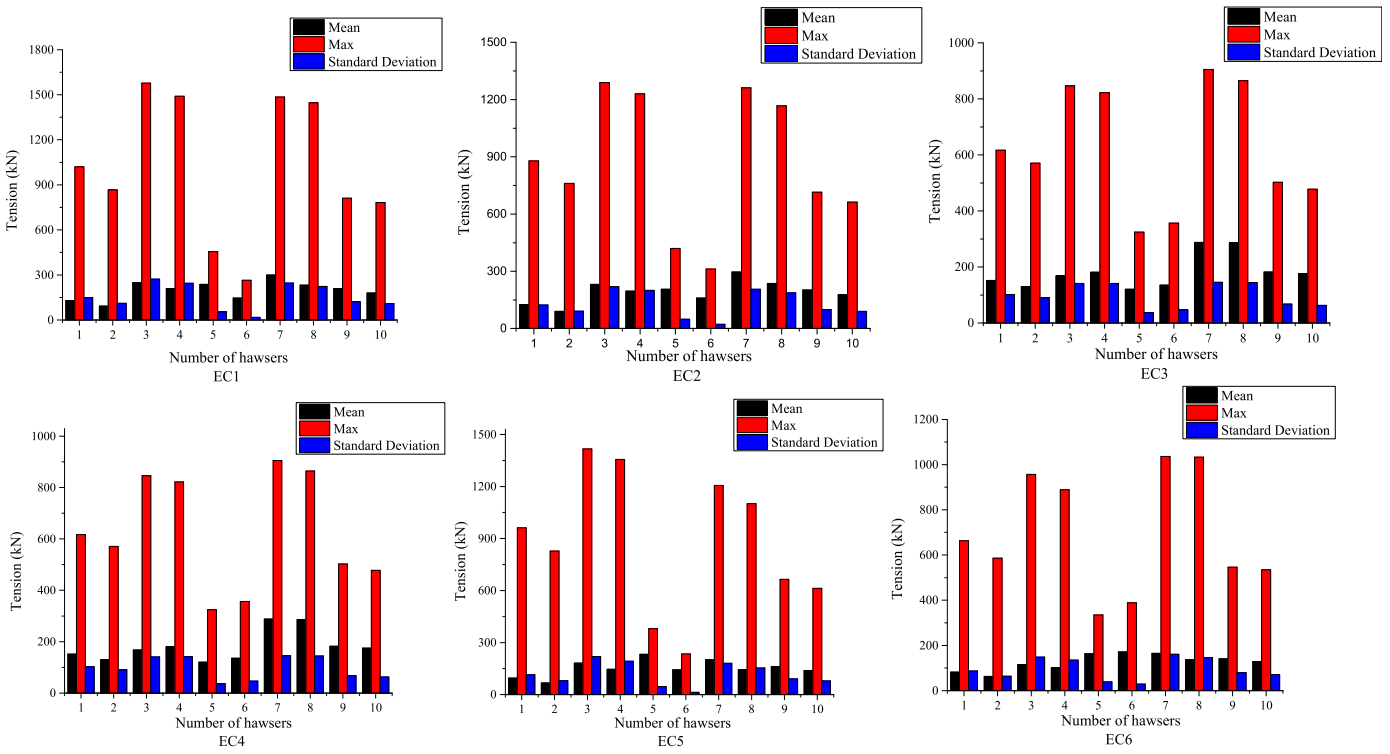

Fig. 7. Statistical characteristics of hawsers tension under different environmental conditions.

process components $X_1(t)$ and $X_2(t)$ with $p_{X_1} = p_{X_2}$. This paper is focused on the latter alternative, i.e. case when processes $X_1(t)$ and $X_2(t)$ are equally distributed. Therefore the current study goal would be, given directly estimated distribution p_X as in option A), to find component distribution p_{X_1} such that

$$p_X = conv\left(p_{X_1}, p_{X_1}\right) \tag{5}$$

thus restricting this study only to a deconvolution case.

5.1. Discrete convolution

This section briefly discusses common knowledge regarding the discrete convolution of two vectors. The convolution of two vectors, $\boldsymbol{u}$ and $\boldsymbol{v}$, represents the area of overlap under vector components, as $\boldsymbol{v}$ slides across $\boldsymbol{u}$. Algebraically, convolution is equivalent to multiplying polynomials whose coefficients are the elements of $\boldsymbol{u}$ and $\boldsymbol{v}$.

Let $m = length(\boldsymbol{u})$ and $n = length(\boldsymbol{v})$. Then $\boldsymbol{w}$ is the vector of length $m + n - 1$, whose k-th element is

$$w(k) = \sum_{j=1}^{m} u(j)v(k-j+1) \tag{6}$$

The sum is over all the values of j that lead to legal subscripts for $u(j)$ and $v(k-j+1)$, specifically $j = max(1, k+1-n) : 1 : \min(k, m)$. When $m = n$, as will be the main case in this paper, the latter gives

$$\begin{aligned} w(1) &= u(1) \bullet v(1) \\ w(2) &= u(1) \bullet v(2) + u(2) \bullet v(1) \\ w(3) &= u(1) \bullet v(3) + u(2) \bullet v(2) + u(3) \bullet v(1) \\ w(n) &= u(1) \bullet v(n) + u(2) \bullet v(n-1) + \ldots + u(n) \bullet v(1) \\ w(2n-1) &= u(n) \bullet v(n) \end{aligned} \tag{7}$$

From Eq. (7) one can also observe that having found $\boldsymbol{u} = \boldsymbol{v} = (u(1), .., u(n))$, one can obtain gradually reduced parts of $\boldsymbol{w}$-components $w(n+1), .., w(2n-1)$, as the index increases from $n+1$ to $2n-1$. The latter clearly would extend vector $\boldsymbol{w}$ into a support domain that is twice as long as the original distribution support domain, i.e. doubling the p_X distribution support length $(2n-1) \bullet \Delta x \approx 2n \bullet \Delta x = 2X_L$, as compared to the original distribution support length $n \bullet \Delta x = X_L$ with Δx being the constant length of each discrete distribution bin. In other words, convolution might potentially convect distribution tail properties farther "downstream," or deeper inside the tail.

Note that $\boldsymbol{w} = (w(1), .., w(n))$ is a discrete representation of the empirical target distribution p_X from the previous section, and n representing the length of distribution support $[0, X_L]$, for simplicity in this paper, one is limited to the case of one-sided positive valued random variables, i.e. $X \geq 0$.

Further in this paper, only the deconvolution case will be studied, i.e. in Eq. (5), will be $\boldsymbol{u} = \boldsymbol{v}$. Note that according to Eq. (6), p_X and p_{X_1} will be distributions corresponding to vectors $\boldsymbol{w}$ and $\boldsymbol{u}$, respectively.

From Eq. (1) is clear that given $\boldsymbol{w} = (w(1), .., w(n))$ one can sequentially find unknown components $\boldsymbol{u} = \boldsymbol{v} = (u(1), .., u(n))$, starting from the first component $u(1) = \sqrt{w(1)}$, then the second $u(2) = \frac{w(2)}{2u(1)}$, and so on until $u(n)$.

As will be further discussed in this paper, authors suggest simple linear extrapolation of self-deconvoluted vector $(u(1), .., u(n))$ towards $(u(n+1), .., u(2n-1))$ In other words p_{X_1} will have its tail linearly extrapolated in the range $(X_L, 2X_L)$. Note that, p_{X_1} can be referred to as the deconvoluted distribution, which is represented in discrete form by the estimated vector $\boldsymbol{u}$. Using Eq. (7), the original vector $\boldsymbol{w}$ will be clearly extended and extrapolated into a support domain that is twice longer than the original distribution support domain, i.e. doubling the p_X distribution support length $(2n-1) \bullet \Delta x \approx 2n \bullet \Delta x = 2X_L$, as compared to the original distribution support length $n \bullet \Delta x = X_L$.

The original data distribution tail, obtained either by measurements or Monte Carlo simulations, is obviously not smooth – the smoothing tail procedure is introduced. To smoothen the original distribution $p_X(x)$ tail, authors have performed smoothening p_X tail interpolation as CDF distribution tail is generally quite regular for high tail values x. More

specifically, Naess-Gaidai (NG) method was used: for $x \geq x_0$, tail behaves very closely like $exp\{-(ax+b)^c+d\}$ with a, b, c, d being suitable constants for the suitable x_0, see next section. Next, linear extrapolation of p_{X_1} tail has been viewed by authors as the most straightforward, unbiased choice. At the same time, other nonlinear extrapolation approaches can easily plug into the proposed method, but then certain assumptions and biases would be introduced.

To summarize, deconvolution being a functional operator, solving functional equation $Y = X * X \equiv conv(X, X)$ with known distribution Y and unknown X. Deconvolution operation can improve the prediction accuracy, since de-convoluted function X exhibits more linear tail behaviour than then original probability distribution function Y.

5.2. Nonlinear duffing oscillator

This section uses a nonlinear Duffing oscillator subjected to Gaussian white noise as an example to showcase the proposed method. Mean up-crossing rate ν_X of the Duffing oscillator response to a stochastic loading was chosen as a target function f_X to study its distribution tail properties, similar to the previous section. Note that in this case f_X is not a probability distribution, but it is a scaled mean up-crossing rate function, which is, of course, closely related to extreme response statistics.

As the first example system, we shall use the ubiquitous single-degree-of-freedom Duffing oscillator excited by the stationary Gaussian white noise W(t)

$$\mathrm{E[W\backslash(t\backslash)W\backslash(t+v\backslash)]} = \delta\backslash(\tau) \tag{8}$$

with $\delta(\tau)$ being δ-function. That is, Duffing oscillator equation takes the specific form

$$\ddot{X} + \beta\dot{X} + X + \varepsilon X^3 = \mathrm{W(t)} \tag{9}$$

where for the present example $\varepsilon = 1, \beta = 0.2$ were chosen. Such a choice of ε makes the Duffing oscillator strongly nonlinear. The attraction of this model for illustration purposes is the fact that the mean level up-crossing rate is known in closed form (later in this paper called « analytic solution»). It thus offers an easy way of verifying the extrapolation approach.

Fig. 8 presents on the left: NG fit of MC simulated Duffing response; on the right: deconvoluted distribution, linearly extrapolated versus analytic solution. It is clearly seen that the deconvoluted function f_{X_1} is more linear in the tail than original target function f_X.

Fig. 9 presents the comparison between the deconvolution method, analytic and NG for the target function f_X.It is clearly seen that suggested deconvolution method performs significantly better than NG extrapolation.

6. Results and discussions

This paper presents the methodology for estimating the FPSO hawser tension. The novel deconvolution method is presented in previous sections [10,18–34]. The suggested technique delivers an accurate extreme value prediction, leveraging all available data effectively. Based on the overall performance of the suggested technique, it was determined that the innovative deconvolution method could include environmental information and produce more robust and accurate predictions based on correct numerical simulations. For a detailed definition of NG functions, [11,4].

Fig. 10 illustrates the final unscaled findings of the deconvolution approach described in this study for the hawser H3 tension, namely the «shorter » decimal log scale f_X tail, extrapolated by deconvolution in addition to a "longer" data distribution tail and NG extrapolation. The « shorter » data set was made 500 times shorter than the full « longer » MC simulated data set, and equidistant sampling was used.

It should be noted that for the FPSO hawser tension data set, it is impossible to draw a robust conclusion regarding the accuracy of the proposed deconvolution method; however, it is seen from Fig. 10 that the proposed method agrees well with the NG method, being based on the «shorter » data set, and delivering distribution quite close to the one based on the directly MC simulated « longer » data set.

7. Conclusions

In this article, the hydrodynamic performance of an FPSO vessel during side-by-side offloading operations in moderate sea conditions has been investigated. In particular, the relative movements between the FPSO and the shuttle tanker, and hawsers tensions have been numerically modelled. The provided research illustrates the practical benefits of using the unique deconvolution technique. As opposed to the majority of engineering fit techniques, the suggested approach is based on the inherent qualities of the underlying data set. It does not presume any extrapolation functional class. The proposed method's prediction accuracy has been validated by comparing direct Monte Carlo simulation and the Naess-Gaidai extrapolation method. Predictions based on the Naess-Gaidai method were found to be consistent with the suggested deconvolution method for simulated hawser tensions.

Since the suggested technique may be deemed unbiased with respect to any pre-selected fitting functional class, the proposed extrapolation method can be used in engineering design, where a more precise unbiased characteristic design value is essential. Also, note that the proposed technique is not limited to only extreme FPSO response prediction, thus having a rather general potential area of engineering applications.

Author credit statement

All authors contributed equally.

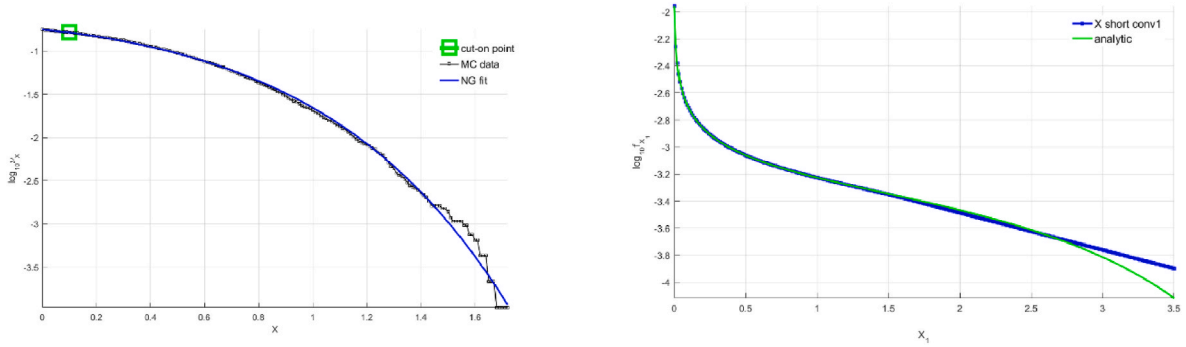

Fig. 8. Left: NG fit of MC simulated Duffing response for f_X. Right: Deconvoluted distribution, linearly extrapolated (blue) f_{X_1} versus analytic solution (green). (For interpretation of the references to colour in this figure legend, the reader is referred to the Web version of this article.)

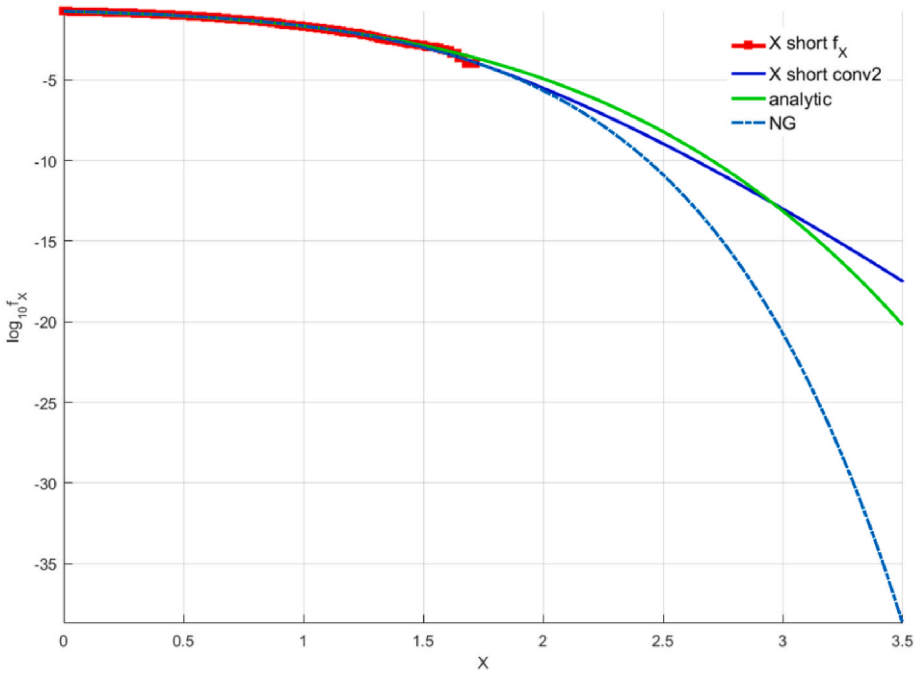

Fig. 9. Comparison between the deconvolution method (solid blue), analytic (green) and NG (dashed blue). MC simulated response is indicated in red (*). (For interpretation of the references to colour in this figure legend, the reader is referred to the Web version of this article.)

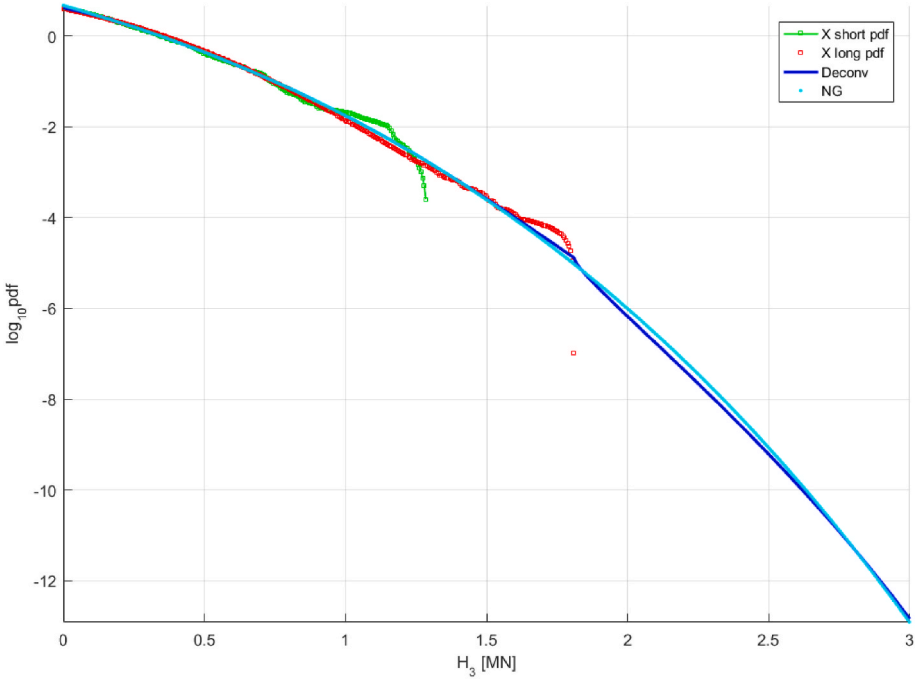

Fig. 10. Response predictions for hawser tension H_3. Unscaled « shorter » decimal log scale f_X tail, raw (green) and extrapolated by deconvolution (solid blue line, along with «longer » data (red line) and NG (cyan line).

Declaration of competing interest

The authors declare that they have no known competing financial interests or personal relationships that could have appeared to influence the work reported in this paper.

Data availability

Data will be made available on request.

Acknowledgement

The authors declare no conflicts of interest. No funding was received.

References

[1] A. Naess, O. Gaidai, A. Batsevych, Prediction of extreme response statistics of narrow-band random vibrations, J. Eng. Mech. 136 (3) (2010) 290–298.
[2] A. Naess, C. Stansberg, O. Gaidai, R. Baarholm, Statistics of extreme events in airgap measurements, J. Offshore Mech. Arctic Eng. 131 (2009).

[3] A. Naess, O. Gaidai, Estimation of extreme values from sampled time series, Struct. Saf. 31 (4) (2009) 325–334.
[4] A. Naess, O. Gaidai, Monte Carlo methods for estimating the extreme response of dynamical systems, Journal of Engineering Mechanics, ASCE 134 (8) (2008) 628–636.
[5] http://www.globalwavestatisticsonline.com/.
[6] AQWA theory manual, Release 15.0, ANSYS, Inc, 2013.
[7] BV, Bureau Veritas, NR 493, Classification of Mooring Systems for Permanent Offshore Units, 2012.
[8] Design, API, Analysis of Station Keeping Systems for Floating Structures: API RP 2SK, API, Washington DC, 2005.
[9] X. Xu, O. Gaidai, A. Naess, P. Sahoo, Improving the prediction of extreme FPSO hawser tension, using another highly correlated hawser tension with a longer time record, Appl. Ocean Res. 88 (2019) 89–98.
[10] Y. Xing, O. Gaidai, Y. Ma, A. Naess, F. Wang, A novel design approach for estimation of extreme responses of a subsea shuttle tanker hovering in ocean current considering aft thruster failure, Appl. Ocean Res. 123 (2022), https://doi.org/10.1016/j.apor.2022.103179.
[11] A. Naess, T. Moan, Stochastic Dynamics of Marine Structures, Cambridge University Press, 2013.
[12] W.G. Price, R.E.D. Bishop, Probabilistic Theory of Ship Dynamics, Chapman and Hall, London, 1974.
[13] O. Gaidai, X. Xu, A. Naess, Y. Cheng, R. Ye, J. Wang, Bivariate Statistics of Wind Farm Support Vesselmotions while Docking", Ships and Offshore Structures, 2020, https://doi.org/10.1080/17445302.2019.1710936.
[14] O. Gaidai, X. Xu, J. Wang, Y. Cheng, R. Ye, O. Karpa, SEM-REV offshore energy site wind-wave bivariate statistics, Renew. Energy 156 (2020) 689–695.
[15] H. Gao, O. Gaidai, A. Naess, G. Storhaug, X. Xu, Improving container ship panel stress prediction, based on anotherhighly correlated panel stress measurement, Mar. Struct. (2018), https://doi.org/10.1016/j.marstruc.2018.11.007.
[16] O. Gaidai, A. Naess, X. Xu, Y. Cheng, Improving extreme wind speed prediction based on a short data sample,using a highly correlated long data, J. Wind Eng. Ind. Aerod. (2019), https://doi.org/10.1016/j.jweia.2019.02.021.
[17] O. Gaidai, A. Naess, O. Karpa, Y. Cheng, R. Ye, Improving Extreme Wind Speed Prediction for North Sea Offshore Oil and Gasfields, 2019, https://doi.org/10.1016/j.apor.2019.04.024.
[18] O. Gaidai, F. Wang, Y. Wu, Y. Xing, A. Medina, J. Wang, Offshore renewable energy site correlated wind-wave statistics, Probabilist. Eng. Mech. 68 (2022), https://doi.org/10.1016/j.probengmech.2022.103207.
[19] J. Sun, O. Gaidai, F. Wang, A. Naess, Y. Wu, Y. Xing, E. van Loon, A. Medina, J. Wang, Extreme riser experimental loads caused by sea currents in the Gulf of Eilat, Probabilist. Eng. Mech. 68 (2022), https://doi.org/10.1016/j.probengmech.2022.103243.
[20] X. Xu, F. Wang, O. Gaidai, A. Naess, Y. Xing, J. Wang, Bivariate statistics of floating offshore wind turbine dynamic response under operational conditions, Ocean Eng. 257 (2022), https://doi.org/10.1016/j.oceaneng.2022.111657.
[21] O. Gaidai, Y. Xing, F. Wang, S. Wang, P. Yan, A. Naess, Improving extreme anchor tension prediction of a 10-MW floating semi-submersible type wind turbine, using highly correlated surge motion record, Front. Mech. Eng. 51 (2022), https://doi.org/10.3389/fmech.2022.888497.
[22] O. Gaidai, Y. Xing, X. Xu, COVID-19 epidemic forecast in USA East coast by novel reliability approach, Research square (2022), https://doi.org/10.21203/rs.3.rs-1573862/v1.
[23] X. Xu, Y. Xing, O. Gaidai, K. Wang, K. Patel, P. Dou, Z. Zhang, A novel multi-dimensional reliability approach for floating wind turbines under power production conditions, Front. Mar. Sci. (2022), https://doi.org/10.3389/fmars.2022.970081.
[24] O. Gaidai, Y. Xing, R. Balakrishna, Improving extreme response prediction of a subsea shuttle tanker hovering in ocean current using an alternative highly correlated response signal, Results in Engineering (2022), https://doi.org/10.1016/j.rineng.2022.100593.
[25] Y. Cheng, O. Gaidai, D. Yurchenko, X. Xu, S. Gao, Study on the dynamics of a payload influence in the polar ship, in: The 32nd International Ocean and Polar Engineering Conference, 2022. Paper Number: ISOPE-I-22-342.
[26] O. Gaidai, G. Storhaug, F. Wang, P. Yan, A. Naess, Y. Wu, Y. Xing, J. Sun, On-board trend analysis for cargo vessel hull monitoring systems, in: The 32nd International Ocean and Polar Engineering Conference, 2022. Paper Number: ISOPE-I-22-541.
[27] O. Gaidai, X. Xu, A. Naess, Y. Cheng, R. Ye, J. Wang, Bivariate statistics of wind farm support vessel motions while docking, Ships Offshore Struct. 16 (2) (2020) 135–143.
[28] O. Gaidai, S. Fu, Y. Xing, Novel reliability method for multidimensional nonlinear dynamic systems, Mar. Struct. 86 (2022), https://doi.org/10.1016/j.marstruc.2022.103278.
[29] O. Gaidai, P. Yan, Y. Xing, A novel method for prediction of extreme wind speeds across parts of Southern Norway, Front. Environ. Sci. (2022), https://doi.org/10.3389/fenvs.2022.997216.
[30] O. Gaidai, P. Yan, Y. Xing, Prediction of extreme cargo ship panel stresses by using deconvolution, Front. Mech. Eng. (2022), https://doi.org/10.3389/fmech.2022.992177.
[31] R. Balakrishna, O. Gaidai, F. Wang, Y. Xing, S. Wang, A novel design approach for estimation of extreme load responses of a 10-MW floating semi-submersible type wind turbine, Ocean Eng. 261 (2022), https://doi.org/10.1016/j.oceaneng.2022.112007.
[32] O. Gaidai, P. Yan, Y. Xing, J. Xu, Y. Wu, A Novel Statistical Method for Long-Term Coronavirus Modelling", F1000 Research, 2022. https://orcid.org/0000-0003-0883-48542.
[33] O. Gaidai, J. Xu, P. Yan, Y. Xing, F. Zhang, Y. Wu, Novel methods for wind speeds prediction across multiple locations, Sci. Rep. 12 (2022), 19614, https://doi.org/10.1038/s41598-022-24061-4.
[34] Gaidai, O., Xing, Y., "Novel reliability method validation for offshore structural dynamic response", Ocean Eng., Vol. 266 (5), https://doi.org/10.1016/j.oceaneng.2022.113016.